Continuum resonance induced electromagnetic torque by a rotating plasma response to static resonant magnetic perturbation field

Yueqiang Liu, J. W. Connor, S. C. Cowley, C. J. Ham, R. J. Hastie et al.

Citation: Phys. Plasmas **19**, 102507 (2012); doi: 10.1063/1.4759205
View online: http://dx.doi.org/10.1063/1.4759205
View Table of Contents: http://pop.aip.org/resource/1/PHPAEN/v19/i10
Published by the American Institute of Physics.

Continuum resonance induced electromagnetic torque by a rotating plasma response to static resonant magnetic perturbation field

Yueqiang Liu,[a] J. W. Connor, S. C. Cowley, C. J. Ham, R. J. Hastie, and T. C. Hender
Euratom/CCFE Fusion Association, Culham Science Centre, Abingdon OX14 3DB, United Kingdom

(Received 14 August 2012; accepted 2 October 2012; published online 17 October 2012)

A numerical study is carried out, based on a simple toroidal tokamak equilibrium, to demonstrate the radial re-distribution of the electromagnetic torque density, as a result of a rotating resistive plasma (linear) response to a static resonant magnetic perturbation field. The computed electromagnetic torque peaks at several radial locations even in the presence of a single rational surface, due to resonances between the rotating response, in the plasma frame, and both Alfvén and sound continuum waves. These peaks tend to merge together to form a rather global torque distribution, when the plasma resistivity is large. The continuum resonance induced net electromagnetic torque remains finite even in the limit of an ideal plasma. [http://dx.doi.org/10.1063/1.4759205]

I. INTRODUCTION

The non-axisymmetric resonant magnetic perturbation (RMP) has been extensively applied in tokamak H-mode plasmas, in order to mitigate the so called type-I edge localized mode (ELM).[1–4] Whilst the ultimate goal of the application of a RMP is to mitigate ELMs, there can be significant side effects on both the plasma confinement and stability, despite the relatively small amplitude of the applied 3D field (of order 10^{-3} of the equilibrium field). Examples of such effects include the experimentally observed density pump out,[3] the change of the toroidal rotation of the plasma due to various torques,[5] the triggering of the finger-like lobes of homoclinic tangles near the X-point, observed in a divertor plasma,[6] and the modification of magnetohydrodynamic (MHD) instabilities due to the presence of a 3D field.[7] It is important to notice that these effects are not independent of each other, and they are often, directly or indirectly, related to the ELM mitigation or suppression.

In this work, we investigate one such aspect, namely, the generation of the resonant electromagnetic torque, as a result of the response of a rotating plasma to a static RMP field. The electromagnetic torque usually acts as a momentum sink term for the toroidal flow of the plasma. The physics of the electromagnetic torque is well understood in the resistive MHD layer theory.[8,9] However, it is less well understood when resonances occur between the plasma response and the continuum waves in the plasma, such as the shear Alfvén and sound waves. Such resonances do not happen if the plasma response (e.g., a magnetic island of finite size) rotates together with the plasma. However, in cases where the plasma response can be approximated as a linear response (e.g., when the magnetic island is suppressed by fast plasma flow), such resonances do occur. This is because the (steady state) plasma response, being locked to the external dc field, rotates in the plasma frame and, hence, is subject to continuum resonances. We mention that the occurrence of the Alfvén resonance in the presence of RMP fields was previously discussed for cylindrical plasmas.[10,11]

As we shall show, the continuum resonances can result in two interesting consequences for the $\mathbf{j} \times \mathbf{b}$ torque. One is the radial re-distribution of the torque density, which can have multiple peaks near resonant surfaces. These resonant surfaces are usually located near, but not coincident with, the rational surface (we shall call this the resonant splitting effect). At sufficiently large plasma resistivity and fast flow, these multiple peaks can merge to form a rather global distribution of the electromagnetic torque, contrary to the conventional understanding of the localized $\mathbf{j} \times \mathbf{b}$ torque near the rational surface. The other consequence of the continuum resonances is the generation of a finite net torque even for an ideal plasma. In this case, the finite torque results from the singularities of the (ideal) MHD equations.

The resonant splitting effect only occurs at finite plasma flow. In the limit of a very slow or vanishing flow, the conventional picture for the $\mathbf{j} \times \mathbf{b}$ torque holds, although more complicated MHD physics can still occur in the resistive layer, due to the favorable average curvature induced additional screening effect.[12]

This work studies only the plasma response and the resulting electromagnetic torque in the presence of a finite rotation. Section II briefly describes the computational models. The linear, single fluid, toroidal MHD code MARS-F (Ref. 13) is used for computing the plasma response to the RMP field. Section III reports the computational results. Based on a simple equilibrium, the physics of the resonance induced $\mathbf{j} \times \mathbf{b}$ torque is illustrated. Section IV draws conclusion.

II. FORMULATIONS

A. MARS-F formulation for computing plasma response

In this work, the linear, steady state plasma response to a RMP field is described by the following resistive, single fluid MHD model in a generic toroidal geometry:

[a]Author to whom correspondence should be addressed. Electronic mail: yueqiang.liu@ccfe.ac.uk.

$$\rho(i\omega_{\rm RMP}+in\Omega)\mathbf{v}=-\nabla p+\mathbf{j}\times\mathbf{B}+\mathbf{J}\times\mathbf{b}-\rho[2\Omega\hat{\mathbf{Z}}\times\mathbf{v}+(\mathbf{v}\cdot\nabla\Omega)R^2\nabla\phi], \quad (1)$$

$$(i\omega_{\rm RMP}+in\Omega)\mathbf{b}=\nabla\times(\mathbf{v}\times\mathbf{B})+(\mathbf{b}\cdot\nabla\Omega)R^2\nabla\phi-\nabla\times(\eta\mathbf{j}), \quad (2)$$

$$(i\omega_{\rm RMP}+in\Omega)p=-\mathbf{v}\cdot\nabla P-\Gamma P\nabla\cdot\mathbf{v}, \quad (3)$$

where the solution variables are the perturbed plasma velocity $\mathbf{v}$, the perturbed magnetic field $\mathbf{b}$, the perturbed plasma current $\mathbf{j}\equiv\nabla\times\mathbf{b}$, and pressure p. All the perturbed quantities have an $\exp(in\phi)$ dependence along the geometric toroidal angle ϕ, with n being the toroidal mode number. The equilibrium plasma density, magnetic field, current, and pressure are denoted by ρ, $\mathbf{B}$, $\mathbf{J}$, P, respectively. $\Gamma=5/3$ is the ratio of specific heats. The other equilibrium quantities appearing in the above equations are the plasma major radius R, the unit vector of the vertical direction $\hat{\mathbf{Z}}$, and the plasma resistivity η.

The toroidal plasma flow, with angular frequency Ω, introduces both the Doppler shift and the terms associated with the flow shear. In MARS-F, the RMP field is generated by a set of magnetic coils with a prescribed current density $\mathbf{j}_{\rm RMP}$, which has a frequency $\omega_{\rm RMP}$ and an $\exp(in\phi)$ toroidal phase dependence. For a dc coil current, which is the case considered in this study, $\omega_{\rm RMP}$ vanishes. In order to determine the plasma response, the above MHD equations are solved together with the following coil equation in the vacuum region:

$$\nabla\times\mathbf{b}=\mathbf{j}_{\rm RMP},\quad \nabla\cdot\mathbf{b}=0. \quad (4)$$

B. Resonance conditions with continuum waves

In the case of a dc RMP field, the steady state plasma response rotates in the plasma frame (with the angular frequency Ω). This creates resonances between the plasma response and continuum waves in the plasma, including both the shear Alfvén wave and the sound wave. The resonance conditions are

$$\Omega^2=\omega_a^2\equiv\omega_A^2(m/q-n)^2/(\hat{\rho}F_{PS}),\qquad \Omega^2=\omega_h^2\equiv\omega_a^2V_s^2/(V_s^2+V_A^2/F_{PS}) \quad (5)$$

for the Alfvén and sound waves, respectively, where $V_A\equiv B_0/\sqrt{\rho}$ is the Alfvén speed, with B_0 being the equilibrium magnetic field amplitude at the magnetic axis. $\omega_A\equiv V_{A0}/R_0$, with V_{A0} and R_0 being the Alfvén speed and the plasma major radius, respectively, at the magnetic axis. $V_s\equiv\sqrt{\Gamma P/\rho}$ is the sound speed. $\hat{\rho}\equiv\rho/\rho_0$ is the plasma density ρ normalized by the central value ρ_0. In a toroidal plasma, the Pfirsch-Schlüter inertial enhancement factor F_{PS} also enters into the resonance conditions, via the re-normalization of the Alfvén speed. A simple analytic estimate of the Pfirsch-Schlüter factor is $F_{PS}=1+q^2/(m-1-nq)^2+q^2/(m+1-nq)^2$,[14] where m is the (resonant) poloidal harmonic number and q the safety factor.

The above conditions (5) imply that (usually) two resonant surfaces will appear, near each rational surface $q=m/n$, as a result of either the Alfvén or the sound wave resonances. Therefore, for a finite pressure plasma, we expect to have (usually) 4 resonant surfaces around the single rational surface. The radial separation of these resonant surfaces depends on the amplitude of the toroidal rotation frequency $|\Omega|$.

C. Evaluation of electromagnetic torque

MARS-F adopts a generic toroidal flux coordinate system (s,χ,ϕ), where $s\equiv\sqrt{\psi_p}$ is the square root of the normalized equilibrium poloidal flux ψ_p, and χ is the (generalized) poloidal angle, whose definition depends on the choice of the Jacobian J. The perturbed magnetic field and current have the following contravariant representations:

$$\mathbf{b}=b^1\nabla\chi\times\nabla\phi+b^2\nabla\phi\times\nabla s+b^3\nabla s\times\nabla\chi, \quad (6)$$

$$\mathbf{j}=j^1\nabla\chi\times\nabla\phi+j^2\nabla\phi\times\nabla s+j^3\nabla s\times\nabla\chi. \quad (7)$$

Using the above representation, it is easy to derive the expression for computing the surface-averaged toroidal electromagnetic torque density in the plasma

$$T_{j\times b}\equiv\frac{1}{2J_0}{\rm Re}\oint R\hat{\phi}\cdot\mathbf{j}\times\mathbf{b}^*Jd\chi d\phi=\frac{1}{2J_0}{\rm Re}\oint(j^1b^{2*}-j^2b^{1*})d\chi d\phi=\frac{\pi}{J_0}\oint{\rm Re}(j^1b^{2*}-j^2b^{1*})d\chi, \quad (8)$$

where $J_0\equiv\oint Jd\chi d\phi$, and the symbol * denotes the complex conjugate. Note that the factor of 1/2 in the torque definition comes from the fact that the physical RMP coil current is a real quantity, but represented in MARS-F via a complex representation $I_0\cos(n\phi)=\frac{1}{2}I_0[\exp(in\phi)+\exp(-in\phi)]$.

The net toroidal electromagnetic torque $T_{\rm net}$, acting on the whole plasma column, is the radial integral of the torque density $T_{\rm net}=\int T_{j\times b}J_0ds$. Since the $\mathbf{j}\times\mathbf{b}$ torque density often peaks near resonant surfaces (and there are often large cancellation effects from the radial integration as will be shown later in the numerical example), it is crucial to control the numerical accuracy of the torque computation. One such control is provided by an alternative evaluation of the net torque. Utilizing the relation $\mathbf{j}=\nabla\times\mathbf{b}$, it can be shown[15] that the net torque can also be computed using only the perturbed magnetic field at an arbitrary surface in the vacuum region, enclosing the plasma column (but not enclosing any conducting structures outside the plasma). In the MARS-F representations, we have

$$T_{\rm net}=\pi\oint\frac{R^2}{J}{\rm Re}(b^1b^{3*})d\chi, \quad (9)$$

where the integration is carried out over the poloidal angle χ of the chosen surface in the vacuum region.

III. NUMERICAL RESULTS

A. Equilibrium

With the purpose of clearly illustrating the resonant splitting physics for the electromagnetic torque, we choose a

simple toroidal equilibrium with aspect ratio of 10 and with a circular plasma cross section. The surface averaged toroidal equilibrium current density is specified as a parabolic function of the plasma minor radius $<J_\phi>= J_\phi^0(1-s^2)$. The radial profile of the equilibrium plasma pressure is specified as $P = P_0(1-s^2)^2$. The values for J_ϕ^0 and P_0 are chosen to have the on-axis safety factor of $q_0 = 1.05$ and the normalized plasma pressure $\beta_N = 1.6$. The equilibrium is self-consistently obtained by running a toroidal equilibrium code. The plasma edge q value thus obtained is $q_a = 2.62$. The radial profile of the safety factor is shown in Fig. 1.

For this study, we position an ideal wall at a $1.4a$ minor radius. The RMP coils are located at the $1.2a$ minor radius, near the outboard mid-plane, producing a $n=1$ magnetic perturbation. [The exact geometry of the coils is not important for investigating the resonant splitting effects presented in this work.] The plasma response has only one rational surface, $q=2$, inside the plasma for the chosen equilibrium and the RMP field, as indicated in Fig. 1.

B. Resonance induced torque density distribution

Figure 2 shows one example of the resonant splitting effect for the computed electromagnetic torque density. A uniform plasma rotation frequency is chosen, with $\Omega = 10^{-3}\omega_A$. Figure 2(a) illustrates the resonance conditions, which are satisfied at radial locations where the plasma rotation $|\Omega|$ curve intersects with either the Alfvén frequency $|\omega_a|$ curve or the sound frequency $|\omega_h|$ curve. There are in total 5 resonant surfaces in this example. We point out that, generally, the number of resonant surfaces depends on the radial profiles of the plasma density, pressure, and rotation frequency near the rational surface. Assuming a subsonic flow, the typical number is 4.

Figure 2(b) plots the MARS-F computed, normalized $\mathbf{j}\times\mathbf{b}$ torque density (the amplitude of the torque density is not of primary interest in this study). A uniform plasma resistivity, corresponding to the Lundquist number $S = 10^9$, is assumed. Even though the resonance conditions (5) are

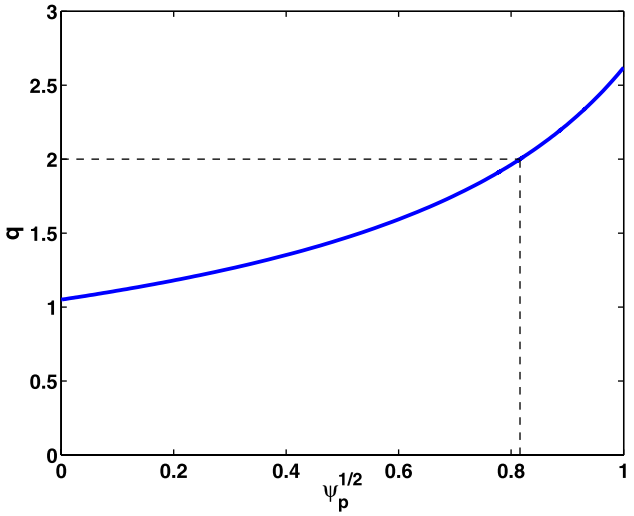

FIG. 1. The radial profile of the safety factor q for the chosen large aspect ratio toroidal equilibrium. The dashed lines indicate the position of the $q=2$ rational surface.

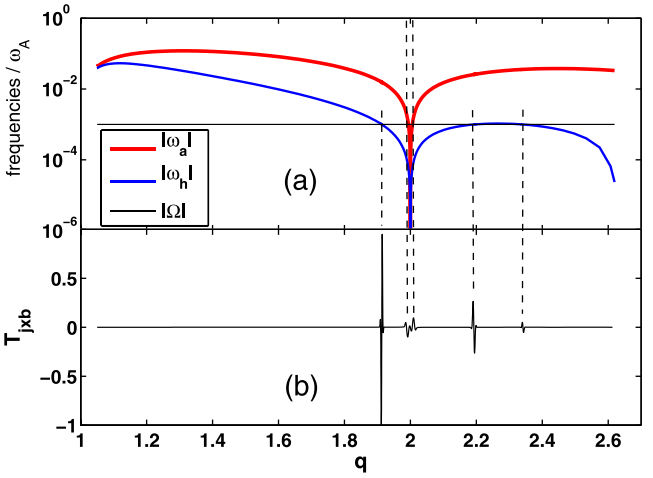

FIG. 2. (a) The radial profiles of the (uniform) plasma rotation frequency $|\Omega|$, the analytic expressions for the Alfvén frequency $|\omega_a|$, and the sound frequency $|\omega_h|$ plotted as functions of the safety factor q. (b) The radial distribution of the computed electromagnetic torque density, with the peak amplitude normalized to unity. The Lundquist number of the plasma is $S = 10^9$.

derived for a straight cylinder, the peak locations of the computed torque density align very well with the analytically predicted locations of the resonant surfaces. We notice a rather significant radial separation of the torque density peaks, resulting from the sound wave resonances.

In the presence of a finite plasma resistivity, the sharp variation of the torque density shown in Fig. 2(b) occurs within the resistive layer of finite width around each resonant surface. This sharp variation is numerically well resolved in MARS-F, as shown by Fig. 3. This is achieved by performing a strong radial mesh packing near the resonant surfaces and by utilizing an *a-posteriori* criterion-based adaptive radial mesh refinement technique that helps to densify the radial mesh points in regions where the computed $\mathbf{j}\times\mathbf{b}$ torque density experiences the sharpest variation. The criterion for the mesh adaptivity combines the amplitude and the curvature (the second derivative) of the torque density curve. Normally, 2-3 iterations of the mesh refinement are sufficient to achieve a good mesh packing for the cases studied here.

It is interesting to note that the radial profile of the torque density has certain parities. In particular, the sound wave continuum resonances (Figs. 3(a), 3(c), and 3(d)) seem to generate odd parity (i.e., anti-symmetric) profiles, whilst the Alfvén continuum resonances (Fig. 3(b), note that two resonant surfaces are present and closely located to each other in this example; another example will be shown in Fig. 9(b) with a larger separation between two Alfvén resonant surfaces) generate even parity (symmetric) profiles. We shall call the odd (even) parity the interchange (tearing) parity. This separation of parities seems to be a generic numerical observation, valid also for other cases studied in this work, and is primarily related to the parities of the perturbed plasma current density near the resonant surfaces. These currents are generated as a result of the plasma response to the RMP field.

Figure 4 shows the radial profiles of the computed perturbed plasma current density. All three components, as defined in Eq. (7), are plotted, together with the parallel

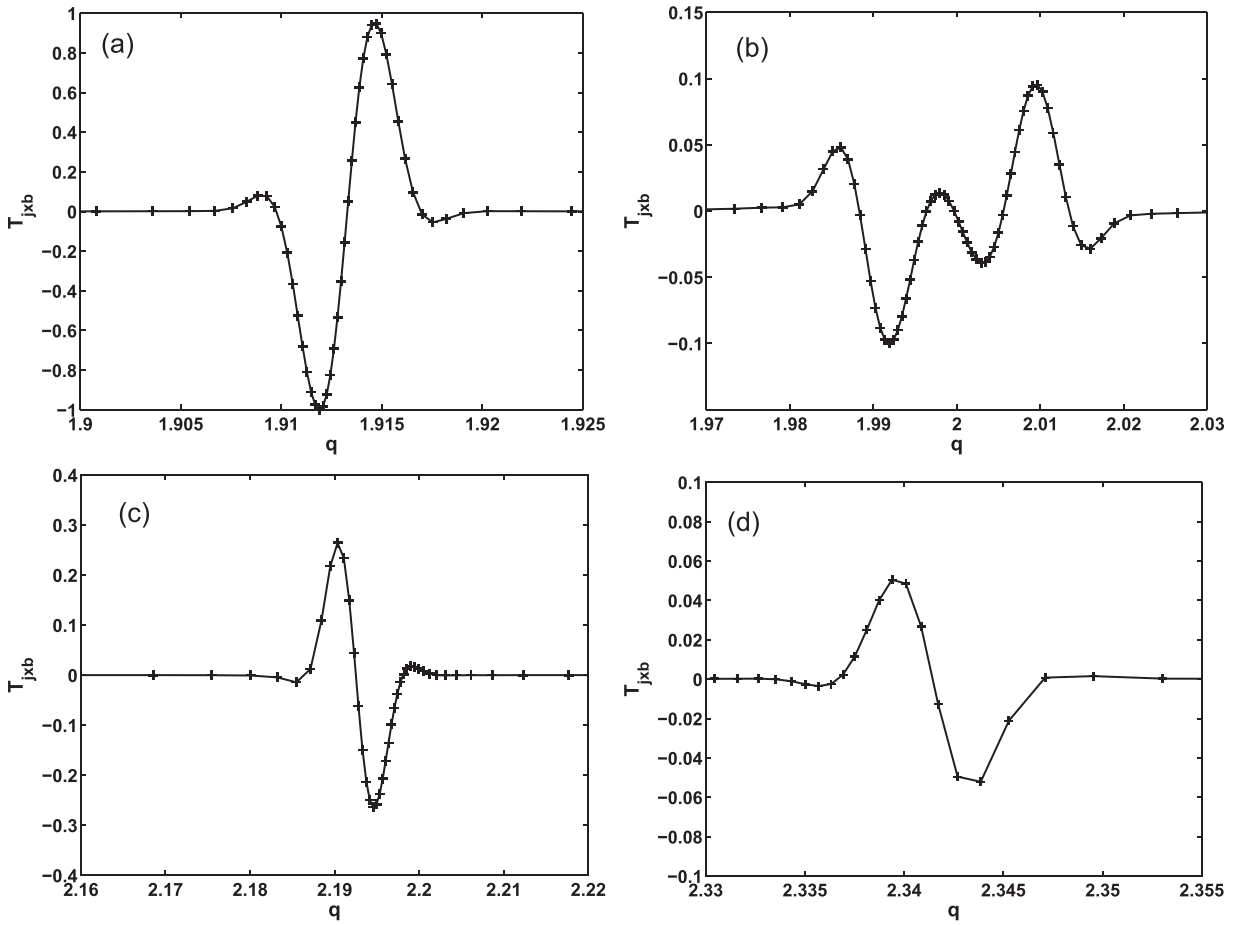

FIG. 3. The detailed radial distribution of the computed electromagnetic torque density as shown in Fig. 2(b), near each resonant surface at (a) $q = 1.9128$, (b) $q = 1.9940$ and 2.0060, (c) $q = 2.1979$, and (d) $q = 2.3420$. The symbols "+" indicate the packed radial mesh.

component $j_{||} \equiv \mathbf{j} \cdot \mathbf{B}/|\mathbf{B}|$, where $\mathbf{B}$ is the equilibrium magnetic field. The perturbed current is generally a complex quantity (in the presence of the plasma flow). Figure 4 shows the components that give the dominant contributions to the electromagnetic torque density. The parity of the current distribution is defined for these components. Again in order to clearly show the splitting effect, we normalize the peak amplitude of each current component to unity. A first observation is that each current component peaks near multiple resonant surfaces, despite the existence of only a single rational surface in our example. These peaks form current sheet-like structures.

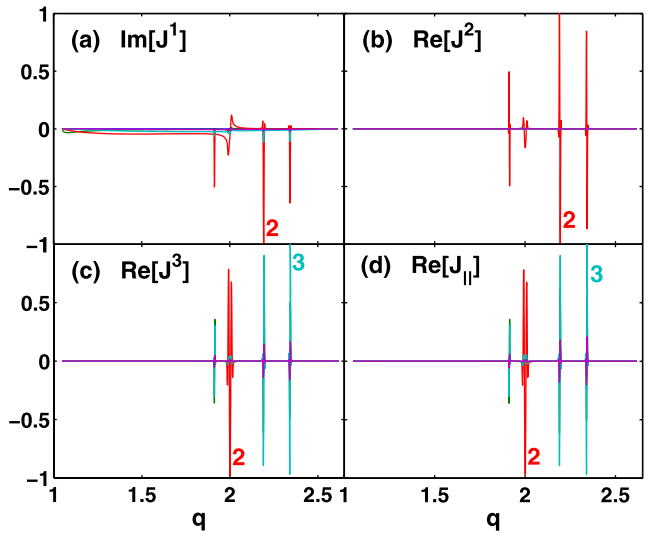

FIG. 4. Radial profiles of the poloidal Fourier harmonics of the computed plasma current perturbations, for (a) radial, (b) poloidal, (c) toroidal, and (d) parallel components, respectively.

The parallel component of the perturbed current, which acts as the major source of the plasma screening of the RMP field, is mainly contributed by the toroidal current perturbation j^3. The radial and poloidal components of the perturbed current, j^1 and j^2, respectively, contribute to the toroidal $\mathbf{j} \times \mathbf{b}$ torque as shown by Eq. (8). A careful examination of the two terms in Eq. (8) reveals that the second term, $j^2 b^{1*}$, gives the dominant contribution to the total torque density. Since, for a resistive plasma response, the perturbed radial field b^1 is almost a constant near each rational surface, the eventual parity of the toroidal $\mathbf{j} \times \mathbf{b}$ torque density is determined by the parity of the perturbed poloidal current component j^2.

Indeed, the perturbed poloidal current j^2 has an interchange type of parity near resonant surfaces created by the sound wave continuum, as shown by the enlarged Figures 5 and 6 (the observation is similar at the resonant surface $q = 2.3420$ but is not shown). On the contrary, the tearing type of parity is created by the Alfvén continuum, as shown by Fig. 7. Similar results for the Alfvén continuum induced

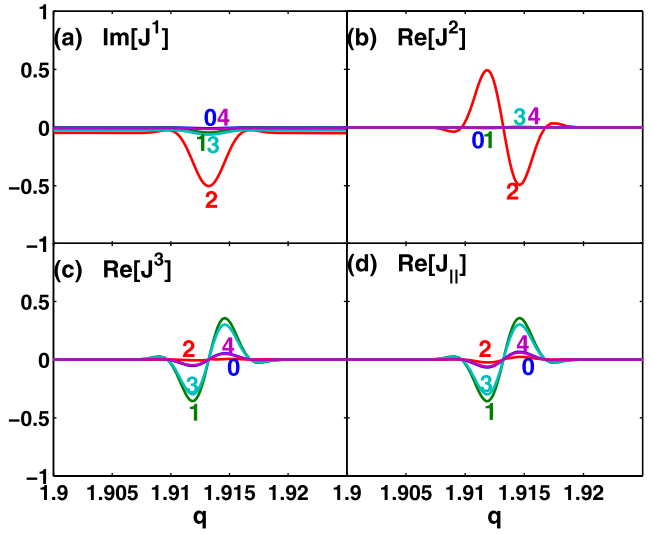

FIG. 5. Radial profiles of the poloidal Fourier harmonics of the computed plasma current perturbations near the first resonant surface $q = 1.9128$, for (a) radial, (b) poloidal, (c) toroidal, and (d) parallel components, respectively.

current splitting and the tearing parity were reported for a cylindrical plasma.[11]

We mention that an odd parity current distribution was reported in our previous work (Fig. 3(b) in Ref. 12), for a case without sound wave contribution and with a very small plasma rotation frequency $\Omega = 10^{-8}\omega_A$. The (Alfvén) resonance splitting effect practically does not occur at this slow flow, as evident from Fig. 2(a). The resulting $\mathbf{j} \times \mathbf{b}$ torque density, though not shown in Ref. 12, follows the same (odd) parity. This odd parity is consistent with the "global" odd parity shown in Fig. 3(b), with respect to the $q = 2$ rational surface, even though the torque density distribution is "locally" close to an even parity with respect to the split (Alfvén) resonant surfaces.

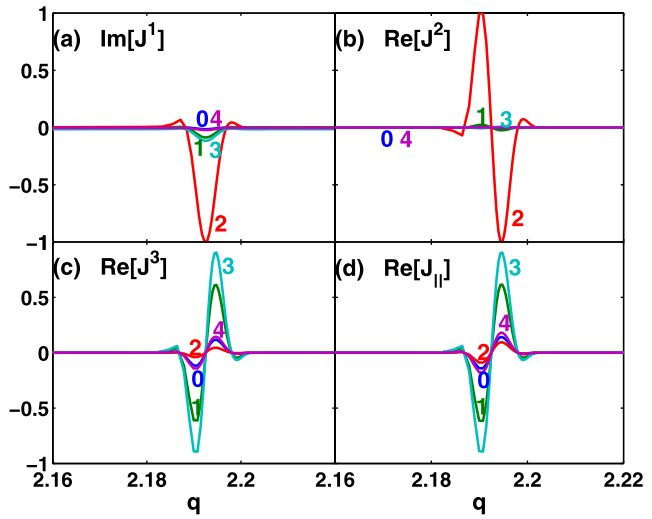

FIG. 6. Radial profiles of the poloidal Fourier harmonics of the computed plasma current perturbations near the fourth resonant surface $q = 2.1979$, for (a) radial, (b) poloidal, (c) toroidal, and (d) parallel components, respectively.

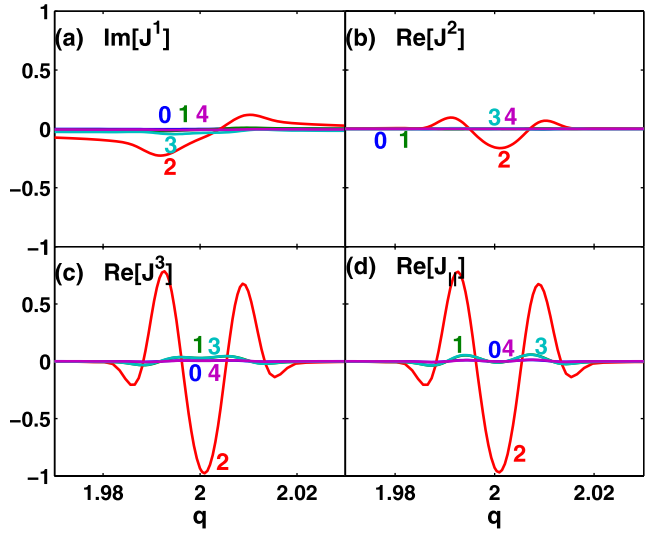

FIG. 7. Radial profiles of the poloidal Fourier harmonics of the computed plasma current perturbations near the second and third resonant surfaces $q = 1.9940$ and 2.0060, for (a) radial, (b) poloidal, (c) toroidal, and (d) parallel components, respectively.

Another qualitative difference between the Alfvén and the sound wave resonances is the poloidal spectrum of the perturbed j^3 (or $j_{||}$). The Alfvén continuum resonance excites mainly the resonant poloidal harmonic $m = 2$ in j^3 (Fig. 7), whilst the sound wave resonance significantly enhances the side-band non-resonant harmonics $m = 1$ and 3. Another possible interpretation is that the sound wave resonance enhances the toroidal coupling of poloidal harmonics for j^3 and $j_{||}$. This enhancement is much less pronounced for the j^1 and j^2 components.

Figure 8 shows the integrated electromagnetic torque $\int_0^s T_{j\times b} J_0 ds$ versus the safety factor q, where $T_{j\times b}$ is shown in Fig. 2(b). A net torque gain is obtained across each resonant surface. In particular, the net gain does not vanish across the sound wave resonant surfaces, despite the anti-symmetric behavior (and hence a significant cancellation) of the torque density.

C. Global distribution of electromagnetic torque density

The strong localization of the electromagnetic torque density and the perturbed plasma current density, shown in the above example, is due to the assumption of a small plasma resistivity (with the Lundquist number of $S = 10^9$). With a larger plasma resistivity (which is often the case in the plasma edge region), the width of the resistive layer around each resonant surface increases. At sufficiently large resistivity, the torque density at multiple resonant surfaces tends to merge, forming a more global radial distribution as shown in Fig. 9(a). Note that at $S = 10^6$, the torque density already becomes reasonably global, despite the presence of only a single rational surface inside the plasma. Increasing the plasma rotation speed leads to further globalization of the torque density profile as shown in Fig. 9(b), due to the increase in the number of resonant surfaces and the increased separation between them. [Note that for the case of $\Omega = 5 \times 10^{-3}\omega_A$ as shown in Fig. 9(b), MARS-F still captures 5

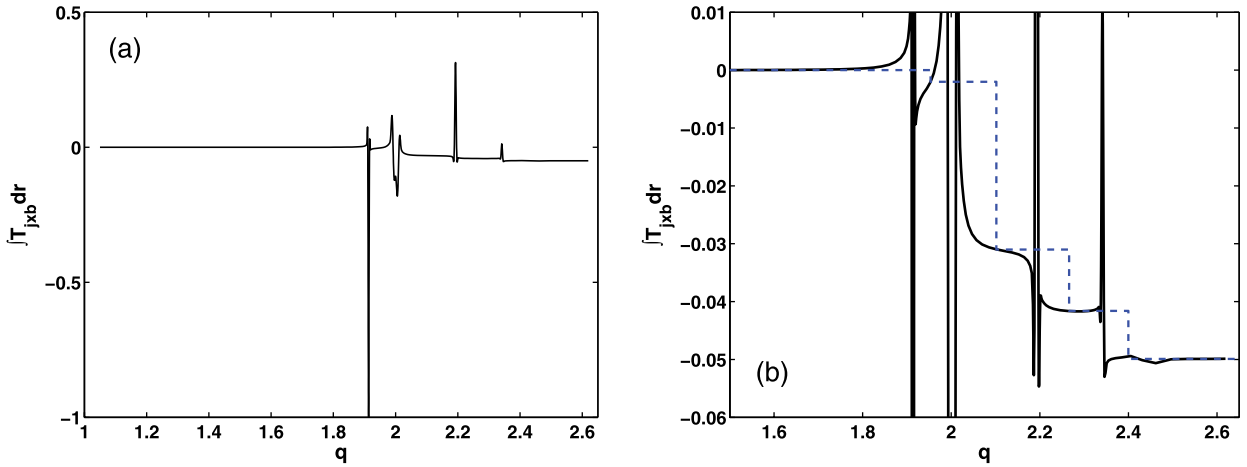

FIG. 8. The integrated electromagnetic torque density across the plasma minor radius with (a) the full profile and (b) the detailed profile near resonant surfaces. The dashed lines indicate the amount of net torque gained while integrating across each resonant surface.

resonant surfaces (2 surfaces due to the Alfvén continuum and 3 surfaces due to the sound continuum), even though the analytic estimate gives only 3 split surfaces for this case. This shows that the analytic estimate is not always accurate in predicting the resonance splitting.]

For a more realistic plasma equilibrium, where many rational surfaces exist inside the plasma and are closely located to each other (typically near the plasma edge, for a divertor plasma), one can expect a rather global $\mathbf{j} \times \mathbf{b}$ torque distribution. One such example was shown in Ref. 16 for a MAST plasma.

D. Finite torque in the ideal plasma limit

The resonances with continuum waves not only redistribute the $\mathbf{j} \times \mathbf{b}$ torque, but can also produce a finite net torque even in the ideal plasma limit (i.e., in a plasma without any dissipation). This has been shown in an analytic calculation based on a slab geometry.[17] The conventional argument, such as the ideal torque balance $\nabla p = \mathbf{j} \times \mathbf{b}$ for vanishing net torque in an ideal plasma, is valid only at the zero-frequency limit. A more fundamental argument for vanishing torque, valid even at finite frequency, is the time reversal symmetry of ideal MHD equations. However, even this argument fails when there are singularities arising from the resonances between the Alfvén[17] or sound wave continuum, and a finite frequency perturbation (in the plasma frame). This is the case for the problem of a rotating plasma response to a static RMP field.

Numerically, we compute the net electromagnetic torque acting on the resistive plasma, while decreasing the plasma resistivity (this requires increasing the radial mesh packing near the split resonant surfaces in order to resolve the layers). Two examples are shown in Figs. 10(a) and 10(b), for fixed plasma rotation frequencies $\Omega = 10^{-3}\omega_A$ and $\Omega = 5 \times 10^{-3}\omega_A$, respectively. The computed net torque indeed approaches a finite value as the Lundquist number S approaches infinity. The numerical accuracy of the net torque computation is verified in Fig. 10(a), where both the volumetric integration method in the plasma and the surface integration method in the vacuum are applied. These two methods were described in Sec. II C. The numerical results agree well.

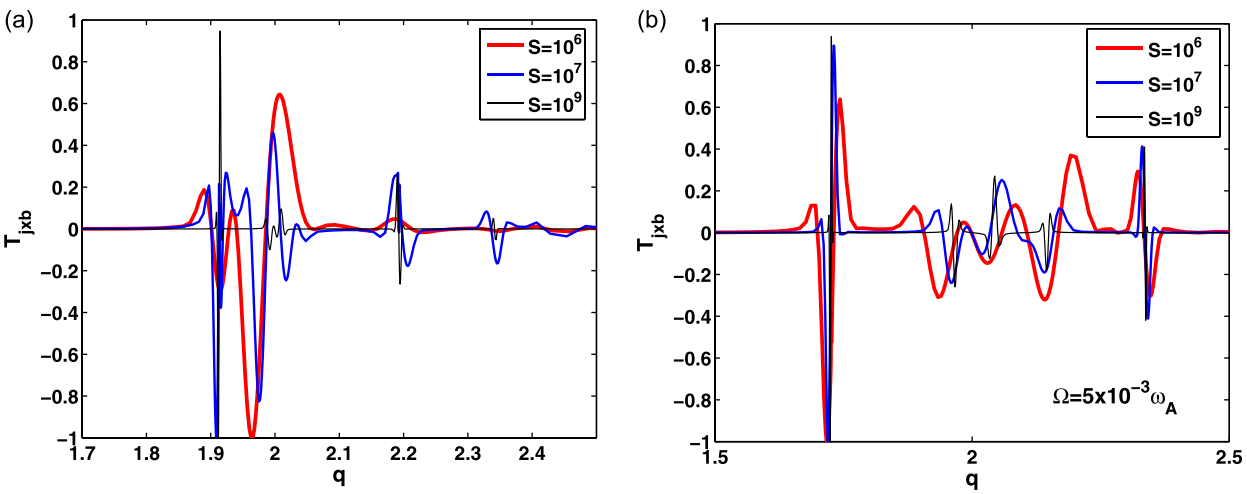

FIG. 9. Radial profiles of the computed electromagnetic torque density with different values of the Lundquist number $S = 10^6, 10^7, 10^9$, for (a) plasma rotation frequency $\Omega = 10^{-3}\omega_A$ and (b) $\Omega = 5 \times 10^{-3}\omega_A$.

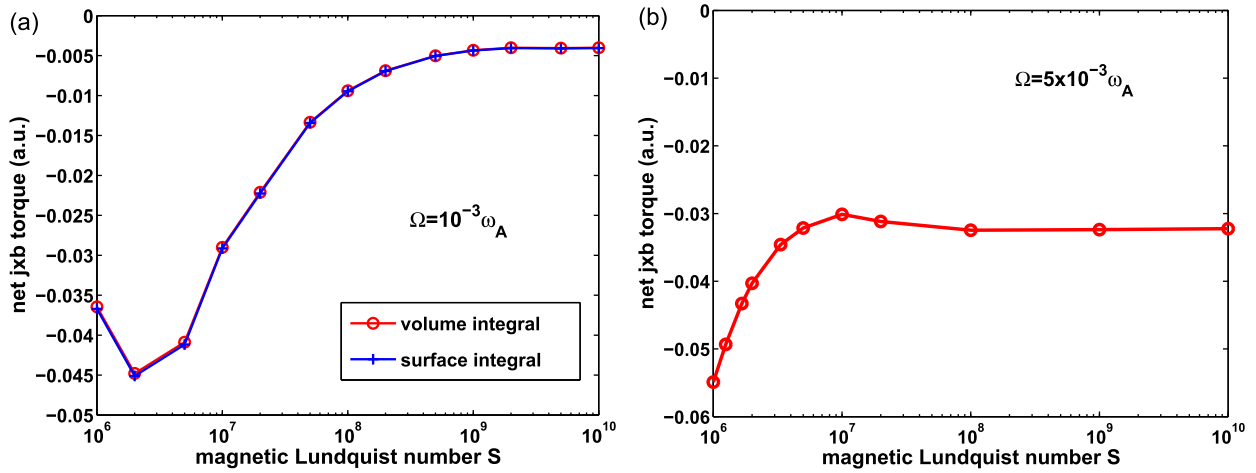

FIG. 10. The computed net electromagnetic torque, acting on the plasma column, versus the magnetic Lundquist number S, for (a) plasma rotation frequency $\Omega = 10^{-3}\omega_A$ and (b) $\Omega = 5 \times 10^{-3}\omega_A$. Both the volumetric integration ("o") and the vacuum surface integration ("+") methods are applied to compute the net torque in (a).

IV. CONCLUSION

The linear, steady state response of a rotating resistive plasma to a static RMP field is subject to resonances with continuum waves, such as the shear Alfvén and the sound waves. This is because the plasma response, being locked to the RMP field, rotates in the plasma frame of reference. As a result of continuum resonances, the perturbed plasma current peaks near several radial locations near a rational surface, effectively splitting the single current sheet, which would have been formed at the rational surface in the absence of continuum resonances, into several current sheets. These multiple current sheets are responsible for the plasma screening of the RMP field. The number of the current sheets is determined by the number of resonant points near each rational surface. Since there are often two resonant points for both Alfvén and sound waves, the total number of current sheets is often 4 for each rational surface.

The same resonant splitting effect results in a radial redistribution of the toroidal electromagnetic $\mathbf{j} \times \mathbf{b}$ torque. The torque density usually peaks near the rational surface in the absence of continuum resonances and has a finite amplitude at several radial locations, corresponding to the resonant surfaces. Moreover, numerical results show that each resonant surface (either Alfvén or sound wave) contributes to the total torque. At sufficiently large plasma resistivity (usually near the plasma edge region), the torque density at adjacent resonant surfaces can merge, forming a rather global radial distribution of the electromagnetic torque density. This is because the width of the resistive layer at each resonant surface increases with increasing plasma resistivity. In the simple numerical example shown here, with only one rational surface inside the plasma, a global electromagnetic torque density already appears at Lundquist number, $S = 10^6$. In a realistic tokamak plasma with a divertor configuration, there are normally many rational surfaces near the plasma edge region. This, combined with the resonant splitting effect, can lead to a global distribution of the electromagnetic torque.

Another important consequence of continuum resonance induced $\mathbf{j} \times \mathbf{b}$ torque splitting is that the net electromagnetic toroidal torque, acting on the whole plasma column, remains finite in the limit of an infinite Lundquist number, i.e., for an ideal plasma. This is associated with the singularities introduced into the ideal MHD solution by continuum resonances, as demonstrated in the analytic work by Taylor.[17] Our toroidal numerical computations confirm this result.

The resonant splitting effect poses computational challenges for toroidal modeling of the RMP penetration into the plasma, since a good numerical resolution is required near each resonant surface, whose radial location depends on the toroidal flow speed of the plasma. In this work, we have utilized an *a-posteriori* criterion based adaptive radial mesh refinement technique.

ACKNOWLEDGMENTS

This work was funded by the RCUK Energy Programme under Grant No. EP/I501045 and the European Communities under the contract of Association between EURATOM and CCFE. The views and opinions expressed herein do not necessarily reflect those of the European Commission.

[1]T. E. Evans, R. A. Moyer, K. H. Burrell, M. E. Fenstermacher, I. Joseph, A. W. Leonard, T. H. Osborne, G. D. Porter, M. J. Schaffer, P. B. Snyder, P. R. Thomas, J. G. Watkins, and W. P. West, Nat. Phys. **2**, 419 (2006).
[2]Y. Liang, H. R. Koslowski, P. R. Thomas, E. Nardon, B. Alper, P. Andrew, Y. Andrew, G. Arnoux, Y. Baranov, M. Bcoulet, M. Beurskens, T. Biewer, M. Bigi, K. Crombe, E. De La Luna, P. de Vries, W. Fundamenski, S. Gerasimov, C. Giroud, M. P. Gryaznevich, N. Hawkes, S. Hotchin, D. Howell, S. Jachmich, V. Kiptily, L. Moreira, V. Parail, S. D. Pinches, E. Rachlew, and O. Zimmermann, Phys. Rev. Lett. **98**, 265004 (2007).
[3]A. Kirk, Y. Q. Liu, E. Nardon, P. Tamain, P. Denner, P. Cahyna, I. Chapman, P. Denner, H. Meyer, S. Mordijck, D. Temple, and MAST Team, Plasma Phys. Controlled Fusion **53**, 065011 (2011).
[4]W. Suttrop, T. Eich, J. C. Fuchs, S. Guenter, A. Janzer, A. Herrmann, A. Kallenbach, P. T. Lang, T. Lunt, M. Maraschek, R. M. McDermott, A. Mlynek, T. Puetterich, M. Rott, T. Vierle, E. Wolfrum, Q. Yu, I. Zammuto, H. Zohm, and ASDEX Upgrade Team, Phys. Rev. Lett. **106**, 225004 (2011).
[5]A. M. Garofalo, W. M. Solomon, J.-K. Park, K. H. Burrell, J. C. DeBoo, M. J. Lanctot, G. R. McKee, H. Reimerdes, L. Schmitz, M. J. Schaffer, and P. B. Snyder, Nucl. Fusion **51**, 083018 (2011).

[6]A. Kirk, J. Harrison, Y. Liu, E. Nardon, I. Chapman, and MAST Team, Phys. Rev. Lett. **108**, 255003 (2012).
[7]I. T. Chapman, R. Scannell, W. A. Cooper, J. P. Graves, R. J. Hastie, G. Naylor, and A. Zocco, Phys. Rev. Lett. **105**, 255002 (2010).
[8]R. Fitzpatrick and T. C. Hender, Phys. Fluids B **3**, 644 (1991).
[9]R. Fitzpatrick, Phys. Plasmas **5**, 3325 (1998).
[10]I. M. Pankratov, A. Ya. Omelchenko, V. V. Olshansky, and K. H. Finken, Nucl. Fusion **44**, S37 (2004).
[11]Y. Kikuchi, K. H. Finken, M. Jakubowski, M. Lehnen, D. Reiser, G. Sewell, and R. C. Wolf, Plasma Phys. Controlled Fusion **48**, 169 (2006).
[12]Y. Q. Liu, J. W. Connor, S. C. Cowley, C. J. Ham, R. J. Hastie, and T. C. Hender, Phys. Plasmas **19**, 072509 (2012).
[13]Y. Q. Liu, A. Bondeson, C. M. Fransson, B. Lennartson, and C. Breitholtz, Phys. Plasmas **7**, 3681 (2000).
[14]C. Wahlberg and A. Bondeson, J. Plasma Phys. **57**, 327 (1997).
[15]V. D. Pustovitov, Nucl. Fusion **47**, 1583 (2007).
[16]Y. Q. Liu, A. Kirk, Y. Sun, P. Cahyna, I. T. Chapman, P. Denner, G. Fishpool, A. M. Garofalo, J. R. Harrison, E. Nardon, and MAST Team, "Toroidal modelling of plasma response and RMP field penetration," Plasma Phys. Controlled Fusion (in press).
[17]J. B. Taylor, Phys. Rev. Lett. **91**, 115002 (2003).